

# Magneto-Transport in the Two-Dimensional Lorentz Gas

A. Kuzmany and H. Spohn

*Theoretische Physik, Ludwig-Maximilians-Universität, Theresienstr. 37, D-80333 München, Germany*  
*email: spohn@stat.physik.uni-muenchen.de, kuzmany@stat.physik.uni-muenchen.de*

(submitted to Physical Review E, September 30, 1997)

We consider the two-dimensional Lorentz gas with Poisson distributed hard disk scatterers and a constant magnetic field perpendicular to the plane of motion. The velocity autocorrelation is computed numerically over the full range of densities and magnetic fields with particular attention to the percolation threshold between hopping transport and pure edge currents. The Ohmic and Hall conductance are compared with mode-coupling theory and a recent generalized kinetic equation valid for low densities and small fields. We argue that the long time tail as  $t^{-2}$  persists for non-zero magnetic field.

PACS number(s): 05.60.+w, 05.20.Dd, 75.50.Jt

## I. INTRODUCTION

Two-dimensional electron films can be manufactured with high perfection in GaAs heterostructures. At low temperatures a mean free path of over  $10^4 nm$  is reached and to a very good approximation the electrons may be considered as noninteracting. To have some interesting physics one nanostructures the probe by lithographic or other techniques. Thereby a strongly repulsive potential is imposed on the electrons with a maximum above the Fermi energy (*quantum antidots*). If the imprinted structure is on a scale larger than the Fermi wave length, adjustable to be of the order of  $50 nm$ , one hopes to capture the transport properties already in the classical approximation.

So far, the most popular geometry has been a regular array of antidots which corresponds classically to the Sinai billard and should result quantum mechanically in the Hofstadter butterfly. The magneto-transport of this periodic structure has been studied in great detail, both experimentally [1–4] and theoretically [5–8]. In our note we investigate randomly placed antidots. To our knowledge, the so far best experimental realization has been achieved by Lütjering [9]. We compare our results with his measurements in the conclusions.

In kinetic theory randomly distributed scatterers are known as the Lorentz gas, which has proved to be an important testing ground. In particular, one can understand precisely the assumptions for the validity of the (linear) Boltzmann equation [10] and check on the accuracy of the low density expansion and its non-analytic character [11–16]. Also the long time tails in the velocity autocorrelation function are seen most convincingly in the Lorentz gas [17]. In distinction from the work mentioned we investigate here the dynamics in presence of a magnetic field perpendicular to the plane of motion.

The model has a strong geometric flavour: one places randomly disks (the scatterers) of radius  $a$  in the plane at density  $n_s$ . The disks may overlap. In the region outside the disks we have independent point particles with

density  $n_e$ . They have mass  $m^*$ , charge  $e$ , and move in a uniform external magnetic field  $B_{ex}$ . Thus a single particle travels along a circle and is elastically reflected upon collision with a scatterer. We denote the velocity of the particle at time  $t$  by  $\mathbf{u}(t)$ . Clearly  $|\mathbf{u}(t)|$  is conserved and we set it equal to the Fermi velocity  $v_F$ , since at low temperatures contributions to the transport only come from the Fermi surface. The radius of gyration is then  $R_e = v_F m^* / e B_{ex}$ .

We are interested in the magneto-transport which relates the steady state current  $\mathbf{j}$  to an in plane uniform electric field  $\mathbf{E}$  by

$$\mathbf{j} = \sigma \mathbf{E} \quad (1.1)$$

for small  $\mathbf{E}$  and want to understand how  $\sigma$  depends on  $B_{ex}$  and  $n_s$ .  $\sigma_{11}$  and  $\sigma_{22}$  are the Ohmic conductivities. In our case  $\sigma_{11} = \sigma_{22}$  by isotropy.  $\sigma_{12} = -\sigma_{21}$  is the Hall conductivity. The magneto-transport will be studied in linear response. This means the dynamics is the one just explained (*zero* electric field) and the transport coefficients are given in terms of the time-integrated velocity autocorrelation functions. Physically one has to average over all of phase space. For a large sample, this is equivalent to fixing the initial position and averaging over the scatterer distribution. It is this prescription we will use both theoretically and in the numerics. Before spelling out the details we introduce dimensionless quantities.

Space is measured in units of the disk radius  $a$  and velocity in units of the Fermi velocity  $v_F$ . The scatterers have then radius 1 and their dimensionless density is  $\rho = n_s a^2$ . The dimensionless radius of gyration is  $R = R_e / a$  and the corresponding magnetic field is  $B = 1/R = ea B_{ex} / v_F m^*$ . Let  $\mathbf{v}(t) = \mathbf{u}(t) / v_F$  be the velocity of the particle at time  $t$  starting at the origin. Clearly  $|\mathbf{v}(t)| = 1$ .  $\mathbf{v}(t)$  depends on  $\mathbf{v}(0)$  and the particular configuration of the scatterers.

We define the dimensionless velocity autocorrelation function by

$$C_{ij}(t) = \langle v_i(0) v_j(t) \rangle, \quad i, j = 1, 2. \quad (1.2)$$

Here  $\langle \cdot \rangle$  is a double average. Firstly there is an average over scatterers. The centers of the disks are distributed according to a Poisson process with uniform density  $\rho$  conditioned on the set  $\{\mathbf{x} \mid |\mathbf{x}| \leq 1\}$  being free of centers. Secondly we average over the initial velocity  $\mathbf{v}(0) = (\cos \varphi, \sin \varphi)$  uniformly in  $\varphi$ . (By rotational invariance this second average could be omitted, but it is of advantage numerically.) The conductivity tensor is then

$$\sigma_{ij} = \frac{n_e e^2}{m^*} D_{ij}, \quad D_{ij} = \int_0^\infty dt \langle v_i(0) v_j(t) \rangle. \quad (1.3)$$

$D$  depends on  $\rho$  and  $B$ . Also of interest is the frequency dependent conductivity defined by

$$\sigma_{ij}(\omega) = \frac{n_e e^2}{m^*} D_{ij}(\omega), \quad D_{ij}(\omega) = \int_0^\infty dt e^{i\omega t} \langle v_i(0) v_j(t) \rangle. \quad (1.4)$$

We note that  $\langle v_i(0) v_j(t) \rangle = \langle v_i(0) v_j(-t) \rangle$  by stationarity and  $\langle v_1(0) v_2(t) \rangle = -\langle v_1(0) v_2(-t) \rangle = -\langle v_2(0) v_1(t) \rangle$  by time reversal. Therefore  $D_{12} = -D_{21}$  and  $D_{ii} = (1/4) \int_{-\infty}^\infty dt \langle \mathbf{v}(0) \cdot \mathbf{v}(t) \rangle$ .

As stated in (1.3) the conductivity is ill-defined. There is always a non-zero probability that the particle will not be scattered at all. If so,  $\langle v_1(0) v_1(t) \rangle = (1/2) \cos(Bt)$  and  $\langle v_1(0) v_2(t) \rangle = (1/2) \sin(Bt)$ , and the time integral in (1.3) needs a reinterpretation. Physically there will always be a weak elastic scattering by impurities, i.e. once in a while the velocity direction is randomized. In approximation the velocity autocorrelation function is then modified to

$$e^{-t/\tau} \langle v_i(0) v_j(t) \rangle \quad (1.5)$$

and the proper definition reads

$$D_{ij}(\omega) = \lim_{\tau \rightarrow \infty} \int_0^\infty dt e^{-t/\tau} e^{i\omega t} \langle v_i(0) v_j(t) \rangle. \quad (1.6)$$

At zero density, no scattering, (1.6) results in

$$D_{11}(\omega) = -i \frac{\omega}{2} \frac{1}{B^2 - \omega^2}, \quad D_{12}(\omega) = \frac{B}{2} \frac{1}{B^2 - \omega^2}, \quad (1.7)$$

as well known from the Drude theory of the Hall effect. In particular, at  $\omega = 0$  both the Ohmic conductivity and the Ohmic resistance vanish.

It is instructive to go back for a moment to the case of an in plane electric field  $\mathbf{E}$ . One finds that for freely moving particles the average current approaches

$$\mathbf{j} = \frac{1}{2B} (-E_2, E_1) \quad (1.8)$$

as  $t \rightarrow \infty$  in accordance with (1.7) at  $\omega = 0$ . In fact, one would expect that scattering cannot make things worse.

Thus for the Lorentz gas there should be a well-defined steady state current  $\mathbf{j}$  for  $B \neq 0$ . We did not find a general argument to establish its existence. The situation at  $B = 0$  is very different. Then the particle is accelerated along the direction of  $\mathbf{E}$ . Since only the velocity direction is randomized by collisions, the energy input from the electric field cannot be dissipated and no meaningful steady state current is reached as  $t \rightarrow \infty$ . However for small  $\mathbf{E}$  the time dependent current settles at a plateau over a time span the longer the smaller  $\mathbf{E}$ , whose value equals  $\sigma \mathbf{E}$  with  $\sigma$  of (1.3).

To give a brief outline: In the following section we discuss the dependence of  $D$  on  $\rho$ ,  $B$  with particular attention to the two percolation thresholds. We also compare our numerics with the mode coupling theory of Götze and Leutheuser [18], which seems to be the only theoretical prediction at intermediate densities. Recently Bobylev et al. [19] derived a generalized transport equation for low scatterer densities and small fields. In the appropriate domain of validity their predictions are in fact very accurate (Section 3), and clearly improve on the phenomenological Boltzmann equation with magnetic field. One of the famous results on the Lorentz gas at  $B = 0$  is the slow decay of the velocity autocorrelation function as  $-t^{-2}$  for large  $t$  in two dimensions [20]. For densities  $\rho < 0.25$  such a power law has been well established numerically [17]. At larger densities there is a pre-asymptotic decay approximately as  $-t^{-1.4}$  and, with reasonable numerical effort, the true asymptotics cannot be seen any more. In Section 4 we argue that also for  $B \neq 0$  the velocity autocorrelation decays as  $t^{-2}$  for large  $t$ . We conclude by a comparison with the experiments of Lütjering and with some comments.

## II. THE STATIC CONDUCTIVITY

To discuss  $D$  in its dependence on  $\rho$ ,  $B$  at zero frequency it is useful to consider first the limiting cases. As explained  $D_{11}(0, B) = 0$ ,  $D_{12}(0, B) = 1/2B$  at  $\rho = 0$ . On the other hand for  $B = 0$  we have  $D_{12}(\rho, 0) = 0$ .  $D_{11}(\rho, 0)$  has been studied numerically [16,17]. For  $\rho \rightarrow 0$  one obtains the Boltzmann value  $D_{11}(\rho) = 3/16\rho$ . Thus close to  $(\rho, B) = 0$ ,  $D$  is somewhat singular and roughly of the form  $(\rho^2 + B^2)^{-1/2}$ . Its precise functional dependence will be discussed in Section 3.

As the density is increased the disks percolate. This means that for  $\rho > \rho_c$ ,  $\rho_c \cong 0.36$  with probability one the origin is contained in a finite domain bounded by scatterers. For  $\rho < \rho_c$  the origin is connected to infinity by a path not intersecting the scatterers. Close to  $\rho_c$  numerically one finds  $D_{11}(\rho, 0) \cong |\rho - \rho_c|^{1.5}$ ,  $\rho \leq \rho_c$ , with no theoretical explanation yet.

In fact, the Lorentz gas has a second percolation threshold. Let us fix  $\rho < \rho_c$  and increase  $B$ . Above some critical value  $B_c$ , the trajectory will either be a circle or skip along a, possibly large, cluster of a finite

number of disks. The bulk current for  $B < B_c$  is reduced to a pure edge current. Since the particle cannot leave a cluster, the mean square displacement is bounded which implies  $D_{11}(\rho, B) = 0$  for  $B > B_c$  by the Einstein relation  $2D_{11} = \lim_{t \rightarrow \infty} \langle \mathbf{r}^2(t) \rangle / 2t$ . A hopping of the particle from cluster to cluster is only possible, if disks with radius  $1 + R$  percolate which means, in our units,  $\rho(1 + R)^2 \geq \rho_c$ , i.e.

$$B_c = \frac{1}{\sqrt{\rho_c/\rho} - 1}. \quad (2.1)$$

Strictly speaking the  $B_c$  of (2.1) is only an upper bound on the true  $B_c$ . One could imagine that already for a slightly smaller  $B$  hopping is suppressed. Numerically, we see a smooth variation through  $B_c$  and such a fine point cannot be decided. In Fig. 1 we plot the two domains in which the Ohmic conductivity vanishes.

The behavior of  $D_{12}$  is somewhat more complicated. We always have the contribution of the circle orbits. According to the Poisson distribution their probability is  $\exp[-\pi\rho\kappa(R)]$  with  $\kappa(R) = R(R + 2)$  for  $R < 1$  and  $\kappa(R) = 4R - 1$  for  $R \geq 1$ . We decompose the average correspondingly as

$$\langle v_i(0)v_j(t) \rangle_{\geq 1} + \langle v_i(0)v_j(t) \rangle_0, \quad (2.2)$$

where  $\langle \cdot \rangle_{\geq 1}$  is the average over all initial  $\mathbf{v}(0)$  and all scatterer configurations such that there is at least one collision for  $0 \leq t < \infty$ . The normalization is  $\langle 1 \rangle_1 = 1 - \exp[-\pi\rho\kappa(R)]$ . If  $\langle v_i(0)v_j(t) \rangle_{\geq 1}$  is absolutely integrable, then

$$D_{ij} = \lim_{t \rightarrow \infty} \langle v_i(0)[x_j(t) - x_j(0)] \rangle_{\geq 1} + (1 - \delta_{ij}) \frac{R}{2} e^{-\pi\rho\kappa(R)}, \quad (2.3)$$

where  $\mathbf{x}(t) = \int_0^t ds \mathbf{v}(s)$  is the position of the particle at time  $t$ . The average  $\langle v_i(0)[x_j(t) - x_j(0)] \rangle_{\geq 1}$  can be further decomposed into averages counting with how many different disks the particle collides in the course of time. The lowest contribution corresponds to the particle skipping around a single disk, etc.. Now, if either  $B > B_c$  or  $\rho > \rho_c$ , then by assumption the sum over all clusters with a *finite* number of disks exhausts already the complete average  $\langle v_i(0)[x_j(t) - x_j(0)] \rangle_{\geq 1}$  for arbitrary  $t$ . (In the domain where  $D_{11} > 0$ , the particle collides with an infinite number of disks). Let us fix then a particular finite cluster of disks and let  $\Gamma$  be the set  $\{\mathbf{x}, \mathbf{v}\}$  of initial conditions such that the particle will eventually collide with each one of the disks in the cluster and no others. By assumption  $|\mathbf{x}| \leq \text{const.}$  for  $\{\mathbf{x}, \mathbf{v}\} \in \Gamma$ . If the dynamics in  $\Gamma$  is mixing (or decomposes into mixing components), then  $\lim_{t \rightarrow \infty} \langle v_1(0)[x_2(t) - x_2(0)] \rangle_\Gamma = \langle v_1(0) \rangle_\Gamma \langle x_2(0) \rangle_\Gamma - \langle v_1(0)x_2(0) \rangle_\Gamma = -\langle v_1(0)x_2(0) \rangle_\Gamma$ , since  $\langle v_1(0) \rangle_\Gamma = \langle \frac{d}{dt} x_1(t) \rangle_\Gamma = 0$  by stationarity.

For one disk the motion is integrable [21] and the mixing assumption fails. In the Appendix we compute the contribution  $D_{12}^{(1)}$ , to (2.3) coming from rosette orbits

around a single disk. The case of two non-overlapping disks was studied in [21]. They still found elliptic islands, however with a small measure already. The mixing assumption seems to be satisfied approximately. One might hope that the remaining contribution,  $-\langle v_1(0)x_2(0) \rangle_\Gamma$ , integrated over allowed scatterer configurations averages to zero. Numerically this does not seem to be the case. At density  $\rho = 0.1$ , the circling and rosette orbits together account only for 50% to the observed  $D_{12}$  in the range  $1.5 \leq B \leq 2.5$ , cf. Fig. 2b.

To have a more complete picture of  $D$  we simulate the Lorentz gas numerically. For given  $B$  and scatterer configuration we compute  $v_j(t)$  up to 60 collision times. The system size is chosen so large that  $\mathbf{x}(t) = \int_0^t ds \mathbf{v}(s)$  never hits the boundary. To speed up the simulation we use a hierarchical search for the next point of collision. For each scatterer configuration we average over 100 randomly chosen initial velocity directions. For  $C_{ij}(t)$  to be sufficiently smooth typically one has to average then over  $10^6$  sample paths. The conductivity is determined from (2.3). In most of parameter space  $\langle v_i(0)x_j(t) \rangle$  has not yet reached its asymptotic value, which reflects the slow decay of the velocity autocorrelation functions. We essentially extrapolate “by hand” to  $t \rightarrow \infty$  which results in a slight overestimate whenever there is an independent check. In Figs. 2-5 we display our results at densities  $\rho = 0.1, 0.15, 0.2$  and  $0.3$ . The percolation threshold is indicated by a vertical line. Note that for  $\rho = 0.1$  the  $B$ -scale starts at  $B = 0.5$ . Our data show a fairly smooth interpolation of the asymptotics at  $B = 0$ ,  $B = \infty$ . The most surprising feature is an initial increase of the Ohmic conductivity with  $B$  at intermediate densities. Apparently, the curved trajectory can bend itself more easily through the dense “labyrinth” of scatterers. The Hall conductivity rises steeply to its maximum and then levels off. The maximum is shifted to smaller  $B$  as the density decreases. In Fig. 2b we insert the contribution of the circling orbits according to (2.3) and of rosette orbits according to (A9).

To our knowledge the only attempt to derive the magneto-conductivity at intermediate densities is the mode coupling theory of Götze and Leutheuser [18]. In Fig. 6 we compare their prediction with our simulation data, note the particular choice of units. For the lowest density,  $\rho = 0.032$ , we find good agreement. Essentially the same behaviour is obtained from the generalized Boltzmann equation, to be discussed in the following section. However, the kinetic theory fails already at density  $\rho = 0.13$  whereas mode coupling is still a reasonable approximation. The next higher density  $\rho = 0.25$  can no longer be accounted for.

### III. LOW DENSITY, SMALL FIELDS

For  $B = 0$  the linear Boltzmann equation is exact at low density. More precisely, for  $\rho \rightarrow 0$  collisions of the

particle with the same scatterer become unlikely and the density of particles in phase space on the scale of the mean free path is governed by the Boltzmann equation. In particular this yields  $D_{11}(\rho, 0) = 3/16\rho$  as  $\rho \rightarrow 0$ . With external magnetic field  $B$  one generalizes in the obvious way to

$$\partial_t f(\mathbf{x}, \varphi, t) = (-\cos \varphi \partial_1 - \sin \varphi \partial_2 - B \partial_\varphi) f(\mathbf{x}, \varphi, t) + 2\rho \int_{-\pi}^{\pi} d\varphi' \frac{1}{4} \sin \left| \frac{\varphi'}{2} \right| [f(\mathbf{x}, \varphi - \varphi', t) - f(\mathbf{x}, \varphi, t)]. \quad (3.1)$$

Here  $f$  is the distribution function at  $\mathbf{x}$ ,  $\mathbf{v} = (\cos \varphi, \sin \varphi)$ ,  $t$ . On the basis of (3.1) one obtains

$$D_{11}^0 = \frac{1}{2} \frac{8\rho/3}{(8\rho/3)^2 + B^2}, \quad D_{12}^0 = \frac{1}{2} \frac{B}{(8\rho/3)^2 + B^2}, \quad (3.2)$$

which we rewrite in scaling form as

$$\begin{aligned} D_{11}^0 &= \frac{1}{\sqrt{\rho^2 + B^2}} g_{11}^0(\rho/B), \\ D_{12}^0 &= \frac{1}{\sqrt{\rho^2 + B^2}} g_{12}^0(\rho/B), \\ g_{11}^0(y) &= \frac{1}{2} \sqrt{1+y^2} \frac{8y/3}{(8y/3)^2 + 1}, \\ g_{12}^0(y) &= \frac{1}{2} \sqrt{1+y^2} \frac{1}{(8y/3)^2 + 1}. \end{aligned} \quad (3.3)$$

For a rigorous derivation the radius of gyration must be of the order of the mean free path. Thus  $B$  must vanish linearly with  $\rho$ . As observed by Bobylev et al. [19] even in the limit  $\rho \rightarrow 0$  some recollisions survive. This is most easily seen for circle orbits with no collisions at all. According to the Boltzmann equation (3.1) even after several turns the particle still has some probability to be scattered. However, for the mechanical Lorentz gas after one completed revolution the annulus is surely free of disks and no scattering events can occur. In [19] the circling orbits and the recollisions are properly taken into account for  $\rho \rightarrow 0$  and a generalized kinetic equation with memory term is derived. On this basis the velocity autocorrelations are computed. The conductivity is still of the scaling form (3.3),

$$\begin{aligned} D_{11}^* &= \frac{1}{\sqrt{\rho^2 + B^2}} g_{11}^*(\rho/B), \\ D_{12}^* &= \frac{1}{\sqrt{\rho^2 + B^2}} g_{12}^*(\rho/B), \end{aligned} \quad (3.4)$$

which is just a consequence of  $B/\rho = \text{const.}$  as  $\rho \rightarrow 0$ . However the scaling functions are now modified to

$$g_{11}^*(y) = \frac{1}{2} \sqrt{1+y^2} \frac{1}{(2y\gamma(x))^2 + 1} (1-x^2) 2y\gamma(x), \quad (3.5)$$

$$g_{12}^*(y) = \frac{1}{2} \sqrt{1+y^2} \frac{1}{(2y\gamma(x))^2 + 1} (1+x^2(2y\gamma(x))^2), \quad (3.6)$$

$$x = e^{-2\pi y}, \quad (3.7)$$

$$\gamma(x) = 1 - \frac{1-x^2}{2x^2} \left( \frac{1-x^2}{2x} \ln \frac{1+x}{1-x} - 1 \right). \quad (3.8)$$

In Fig. 7 we plot  $g_{11}^*$ ,  $g_{12}^*$ . Note that in terms of the polar angle in the  $\rho$ - $B$ -plane the scale is highly compressed at the left. In Fig. 8 we plot the correction to the Boltzmann value (3.3).

Of course,  $D^*$  reproduces the correct limiting behaviour for  $\rho \rightarrow 0$  and  $B \rightarrow 0$ . According to (2.1) the percolation boundary behaves as  $B_c \cong 1.66\sqrt{\rho}$  for small  $\rho$ . Since for the validity of (3.4)  $B$  is scaled proportional to  $\rho$ ,  $D^*$  cannot see this threshold.

In Figs. 9, 10 we compare our numerical results with  $D^*$ . We also include  $D^0$ . As expected,  $D^*$  is a considerable improvement. Note that the agreement is not uniform in  $\sqrt{B^2 + \rho^2}$ . This reflects that at  $B = 0$  the Boltzmann equation has a restricted range of validity, e.g.  $D_{11}(\rho, 0)/D_{11}^0(\rho) = 0.65$  at  $\rho = 0.1$ .

#### IV. VELOCITY AUTOCORRELATIONS

On the level of the linear Boltzmann equation (3.1) one obtains an exponential decay for the velocity autocorrelations. Explicitly

$$C_{11}^0(t) = \frac{1}{2} e^{-|t|/\tau_0} \cos(Bt), \quad C_{12}^0(t) = \frac{1}{2} e^{-|t|/\tau_0} \sin(Bt), \quad (4.1)$$

with  $\tau_0 = (8\rho/3)^{-1}$ . The correct low density/ small field behaviour has a more interesting structure. To state the result it is convenient to introduce the Laplace transforms

$$F(z) = \int_0^\infty dt e^{-zt} 2(C_{11}(t) + iC_{12}(t)) \quad (4.2)$$

for  $\Re(z) > 0$ . In the same approximation as leading to (3.4) one obtains

$$F(z) = \frac{1 - e^{-(z+\nu)T}}{z - i\omega + \nu \int_{-\pi}^{\pi} d\psi g(\psi) \frac{1 - e^{i\psi}}{1 - e^{(z+\nu)T + i\psi}}} + \frac{e^{-(z+\nu)T}}{z - i\omega}. \quad (4.3)$$

We find it convenient to compare the Fourier transforms

$$\hat{C}_{ij}(\omega) = \int_{-\infty}^{\infty} dt e^{-i\omega t} C_{ij}(t) \quad (4.4)$$

with the simulation data. Since  $C_{11}(t)$  is even and  $C_{12}(t)$  is odd, we have  $\hat{C}_{11}(\omega) = \Re(F(i\omega) + F(-i\omega))$ ,  $\hat{C}_{12}(\omega) = i\Re(-F(i\omega) + F(-i\omega))$ . The circle orbits yield  $\delta$ -peaks at  $\omega = \pm 1/R$  with weight  $\exp(-4\pi\rho R)$ . In Fig. 11 we plot the prediction from (4.3) and compare it with the numerics. Note that the  $\delta$ -peaks are out of scale. As anticipated the agreement is excellent, in fact over the whole low density/ small field regime. We plot  $\hat{C}_{12}(\omega)$ , which turns out to be negative, Fig. 12. As the ratio  $\rho/B$  is increased, the characteristic double peak merges into a single peak which shifts then to  $\omega = 0$ .

Away from low density/ small fields we have no theory to compare with. For  $B = 0$   $C_{11}(t)$  has the long time tail of the form  $C_{11}(t) = -\alpha t^{-2}$  with  $\alpha > 0$ . We refer to [18] for a detailed discussion. The heuristic explanation runs as follows: At long times the main contribution of  $C_{11}(t)$  comes from paths returning to the origin at time  $t$ . Let  $\mathbf{v}(0) = (1, 0)$ . Then the particle will be more likely to return from the right which yields a negative correlation in the velocity. For the excursion away from the origin we use a random walk approximation. If at some intermediate time the particle arrives at the line  $x = 0$ , then it will return to the origin equally likely from right and left and the contribution to  $C_{11}(t)$  vanishes. Therefore the tail can be computed from a return to the origin at time  $t$  of a random walker *without* ever hitting the line  $x = 0$ . This probability decays as  $t^{-2}$  in two dimensions. Clearly, in our argument we only used that the motion before returning to the origin is diffusive. This remains valid for non-zero  $B$ . Thus  $C_{11}(t)$  and  $C_{12}(t)$  should have a decay as  $t^{-2}$  for  $t \rightarrow \infty$ . For  $B = 0$  the long time tail is most clearly seen at  $\rho = 0.15$  [17]. We increase  $B$  to 0.2 and average over  $3 \cdot 10^7$  sample paths. The effective exponent for both correlations is 1.9 with a negative prefactor, Fig. 13. However the prefactor of  $C_{11}(t)$  becomes positive in the range  $B = 0.5 \dots 0.8$  and of  $C_{12}(t)$  in the range  $B = 0.6 \dots 3$ . Thus when the particle returns to the origin it picks up more complicated velocity correlations than in the case  $B = 0$ . As one example of such a sign reversal in the 1,2-correlation we display the data for  $\rho = 0.2$ ,  $B = 2.3$ , Fig. 14. The effective exponents are approximately 1.4.

## V. DISCUSSION

We studied transport in the two-dimensional Lorentz gas with a constant magnetic field perpendicular to the plane of motion. The theory of Bobylev et al. is in fair agreement with our simulation data, both for the transport coefficients and the velocity autocorrelations. Away from low density/small magnetic fields there is little theory to compare with. The qualitative properties of the magnetotransport can be guessed from the well understood limiting cases  $B \rightarrow 0$  and  $B \rightarrow \infty$ . The most unexpected feature is an increase in the Ohmic conductivity with increasing  $B$  at intermediate densities. Such

a behavior has also been found experimentally [9].

In these measurements antidots are imprinted at random locations with densities  $1/(1000nm)^2$ ,  $1/(600nm)^2$ ,  $1/(400nm)^2$ ,  $1/(300nm)^2$ , and  $1/(240nm)^2$ , resp. The electrons feel a screened potential. For the periodic case this is usually modelled by  $V(x_1, x_2) = V_0 |\sin(\pi x_1/a) \sin(\pi x_2/a)|^\beta$  with  $\beta$  ranging from 2 to 4. For a random distribution the true potential is more complicated, in particular when there is strong overlap. Thus we cannot expect quantitative agreement between our hard disk model potential and the experiment [9]. There the reduced density roughly ranges from 0.01 to 0.25 in our units. The dimensionless magnetic field varies from 0 to 3. Qualitatively the conductivities  $D_{11}$ ,  $D_{12}$  in dependence on  $B$  follow our curves. However the measured  $D_{12}$  is smaller by approximately a factor 1/2. At the largest density a distinct increase in  $D_{11}$  with  $B$  close to  $B = 0$  is observed. As in our numerical studies the percolation threshold,  $B_c$ , is hardly seen in the Hall conductance. The Ohmic conductivity is small for  $B > B_c$ , but the transition region is fairly broad.

The velocity autocorrelations have a slow decay over the full range of parameters. Presumably it is governed by  $t^{-2}$ , which is however severely masked by an even slower preasymptotic decay. The definite sign of the prefactor at  $B = 0$  is not retained.

## ACKNOWLEDGMENTS

We thank W. Schirmacher for bringing the thesis of G. Lütjering to our attention.

## APPENDIX A: HALL CONDUCTIVITY OF ROSETTE ORBITS

We determine the contribution to  $D_{12}$  from orbits which circle around a single scatterer, cf. Section 2. Since  $B > B_c$ , we discuss only the case  $R < 1$ . There is a corresponding formula for  $R \geq 1$ .

We choose a large square box  $\Lambda$ . Let  $y = \{\mathbf{y}_1, \dots, \mathbf{y}_n\}$  be the centers of the scatterers and  $P_\rho(dy)$  their normalized Poisson distribution at density  $\rho$ . We set  $\Lambda(y) = \{\mathbf{x} \in \Lambda \mid |\mathbf{x} - \mathbf{y}_j| \geq 1, j = 1, \dots, n\}$  and denote by  $|\Lambda(y)|$  the area of this set. Let  $F_j(t; \mathbf{x}, \varphi, y) = \cos \varphi \sin \varphi(t; \mathbf{x}, \varphi, y)$  if  $\varphi(t)$  defines a rosette orbit at scatterer  $j$  and  $F_j = 0$  otherwise. Then

$$\langle v_1(0)v_2(t) \rangle_1 = \int P_\rho(dy) \frac{1}{|\Lambda(y)|} \int_{\Lambda(y)} d^2x \frac{1}{2\pi} \int d\varphi \sum_{j=1}^n F_j(t). \quad (\text{A1})$$

We have  $|\Lambda(y)| \cong |\Lambda|e^{-\pi\rho}$ . By translation symmetry we shift the scatterer  $j$  to the origin and introduce the polar coordinates  $\mathbf{x} = (r \cos \alpha, r \sin \alpha)$ . Let  $f_r(t; \alpha, \varphi) =$

$\cos \varphi \sin \varphi(t; r, \alpha, \varphi)$  if the orbit with initial center of gyration  $(r \cos \alpha, r \sin \alpha)$  and initial velocity  $(\cos \varphi, \sin \varphi)$  defines a rosette orbit around the scatterer located at 0 and  $f_r = 0$  otherwise. Let  $d(y) = \min_j |\mathbf{y}_j|$ . Taking the limit  $|\Lambda| \rightarrow \infty$  we obtain

$$\begin{aligned} \langle v_1(0)v_2(t) \rangle_1 &= \rho e^{\pi \rho} \int P_\rho(dy) \chi\{2 \leq d(y)\} \times \\ &\quad \int_{1-R}^{(1+R) \wedge (d(y)-1-R)} dr r \frac{1}{2\pi} \int d\alpha \int d\varphi f_r(t, \alpha, \varphi) = \\ &\quad \rho e^{\pi \rho} \int P_\rho(dy) \chi\{r + R + 1 \leq d(y)\} \times \\ &\quad \int_{1-R}^{1+R} dr r \frac{1}{2\pi} \int d\alpha \int d\varphi f_r(t, \alpha, \varphi) = \\ &\quad \rho e^{\pi \rho} \int_{1-R}^{1+R} dr r e^{-\pi(r+R+1)^2 \rho} \frac{1}{2\pi} \int d\alpha \int d\varphi f_r(t, \alpha, \varphi) \quad (\text{A2}) \end{aligned}$$

with  $\chi(A)$  denoting the characteristic function of the set  $\{A\}$ .

As before, the Hall conductivity of rosette orbits is given by

$$D_{12}^{(1)} = \lim_{z \rightarrow 0} \int_0^\infty dt e^{-zt} \langle v_1(0)v_2(t) \rangle_1. \quad (\text{A3})$$

By rotation invariance, the  $\alpha$  integration becomes trivial. Thus we have to determine

$$\lim_{z \rightarrow 0} \int_0^\infty dt e^{-zt} \int d\varphi f_r(t; \alpha, \varphi). \quad (\text{A4})$$

We fix  $\alpha = \frac{3\pi}{2}$  and  $r$  such, that  $1 - R \leq r \leq 1 + R$ . Then  $-\varphi_+ \leq \varphi \leq \varphi_+$ , with

$$\varphi_+ = \arccos((1 - R^2 - r^2)/(2Rr)). \quad (\text{A5})$$

$\varphi(t)$  increases linearly in  $t$ . At a collision  $\varphi(t)$  jumps by the angle

$$\Psi = 2 \arccos((r^2 - R^2 - 1)/2R). \quad (\text{A6})$$

Thus

$$\varphi(t) = \varphi + \frac{t}{R} + n(t, \varphi)\Psi, \quad (\text{A7})$$

where  $n(t, \varphi)$  is the number of collisions up to time  $t$  for the initial  $\varphi(0) = \varphi$ . Inserting in (A4) yields

$$\lim_{z \rightarrow 0} \int_0^\infty dt e^{-zt} \int_{-\varphi_+}^{\varphi_+} d\varphi \cos \varphi \sin(\varphi + \frac{t}{R} + n(t, \varphi)\Psi) =$$

$$\begin{aligned} &\lim_{z \rightarrow 0} R \int_{-\varphi_+}^{\varphi_+} d\varphi \cos \varphi (2i(-zR + i))^{-1} \times \\ &\quad [ (e^{\varphi_+(-zR+i)} e^{zR\varphi} - e^{i\varphi}) + (e^{2\varphi_+(-zR+i)} - 1) \times \\ &\quad \sum_{n=0}^{\infty} e^{i(n+1)\Psi} e^{(2n+1)(-zR+i)\varphi_+} e^{zR\varphi} ] + c.c. = \\ &\quad R \int_{-\varphi_+}^{\varphi_+} d\varphi \cos \varphi [ (\cos \varphi - \cos \varphi_+) - \\ &\quad (2(1 - \cos(2\varphi_+ + \Psi)))^{-1} \times \\ &\quad (\cos(3\varphi_+ + \Psi) - \cos(\varphi_+ + \Psi))] = \\ &\quad R(\varphi_+ - \frac{1}{2} \sin 2\varphi_+) + \\ &\quad 2R(\sin \varphi_+)^2 \sin(2\varphi_+ + \Psi)(1 - \cos(2\varphi_+ + \Psi))^{-1}. \quad (\text{A8}) \end{aligned}$$

Combined with (A2) we obtain

$$\begin{aligned} D_{12}^{(1)} &= R \int_{1-R}^{1+R} dr r \rho e^{\pi \rho(1-(r+R+1)^2)} \{ \varphi_+ - \sin \varphi_+ \cos \varphi_+ + \\ &\quad 2(\sin \varphi_+)^2 \cos(\varphi_+ + (\Psi/2)) / \sin(\varphi_+ + (\Psi/2)) \}. \quad (\text{A9}) \end{aligned}$$

In Fig. 2b we plot our result (A9) for  $\rho = 0.1$  as a function of  $B = 1/R$ .

- 
- [1] A. Lorke, J. P. Kotthaus, and K. Ploog, Phys. Rev. **B** **44**, 3447 (1991)
  - [2] K. Ensslin and R. Schuster, in III-IV Semiconductor Quantum Systems, ed. by K. Ploog, Institution of Electrical Engineers, New York, IEE 1996
  - [3] D. Weiss, Phys. Rev. Lett. **66**, 2790 (1991)
  - [4] T. Schlösser, Quantentransport in lateralen Übergittern, Dissertation, Universität München, 1995
  - [5] T. Geisel, A. Zacherl, and G. Radons, Phys. Rev. Lett. **59**, 2503 (1987); Z. Phys. **B** **71**, 117 (1988)
  - [6] R. Fleischmann, T. Geisel, and A. Ketzmerick, Phys. Rev. Lett. **68**, 1367 (1992)
  - [7] M. Fließer, G. J. O. Schmidt, and H. Spohn, Phys. Rev. **E** **53**, 5690 (1996)
  - [8] R. Silberbauer, Quantenmagnetotransport und Quantenchaos in Antidot-Übergittern, Universität Regensburg, 1994
  - [9] G. Lütjering, Nanostrukturierte Antidot-Systeme: vom ballistischen Billard zum Metall-Isolator Übergang, Dissertation, Universität Stuttgart, 1996
  - [10] H. Spohn, Large Scale Dynamics of Interacting Particles, Berlin, Springer 1991
  - [11] M. H. Ernst and A. Weijland, Phys. Rev. **A** **34**, 39 (1971)

- [12] A. Weijland, J. Math. Phys. **15**, 1942 (1974)
- [13] W. Götze, E. Leutheußer, and S. Yip, Phys. Rev. **A 23**, 2634 (1981); **A 24**, 100 (1981); **A 25**, 533 (1982)
- [14] E. Leutheußer, Phys. Rev. **A 28**, 1762 (1983)
- [15] A. J. Masters and T. Keyes, Phys. Rev. **A 26**, 2129 (1982); **A 27**, 2603 (1983)
- [16] B. J. Alder and W. E. Alley, J. Stat. Phys. **19**, 341 (1978)
- [17] C. P. Lowe and A. J. Masters, Physica **A 195**, 149 (1993)
- [18] W. Götze and E. Leutheußer, Z. Physik **B 45**, 85 (1981)
- [19] A. V. Bobylev, F. A. Maaß, A. Hansen, and E. H. Hauge, Phys Rev. Lett. **75**, 197 (1995)
- [20] B. J. Alder and T. E. Wainwright, Phys. Rev. **A 1**, 18 (1970)
- [21] N. Berglund, H. Kunz, J. Stat. Phys. **83**, 81 (1996)

## Figure captions

Fig. 1: The percolation thresholds for the Lorentz gas

Fig. 2: Ohmic conductivity  $D_{11}$  (a) and Hall conductivity  $D_{12}$  (b) as functions of  $B$  for  $\rho = 0.1$  in dimensionless units. (—) is the zero-scatterer contribution of (2.3) and (- - -) is the zero- and one-scatterer contribution of (A9)

Fig. 3: Ohmic conductivity  $D_{11}$  (a) and Hall conductivity  $D_{12}$  (b) as functions of  $B$  for  $\rho = 0.15$  in dimensionless units

Fig. 4: Ohmic conductivity  $D_{11}$  (a) and Hall conductivity  $D_{12}$  (b) as functions of  $B$  for  $\rho = 0.2$  in dimensionless units

Fig. 5: Ohmic conductivity  $D_{11}$  (a) and Hall conductivity  $D_{12}$  (b) as functions of  $B$  for  $\rho = 0.3$  in dimensionless units

Fig. 6a: Ohmic conductivity  $D_{11}$  according to the mode-coupling theory of [18] for various densities

Fig. 6b: Simulation data of the Ohmic conductivity  $D_{11}$  for the same densities and in the same units as Fig. 6a

Fig. 7: The scaling functions  $g_{11}^*$  (a) and  $g_{12}^*$  (b) as functions of  $x = e^{-2\pi\rho/B}$

Fig. 8: The ratios  $D_{11}^*/D_{11}^0$  (a) and  $D_{12}^*/D_{12}^0$  (b) as functions of  $x = e^{-2\pi\rho/B}$

Fig. 9: Inverse Ohmic conductivity  $1/D_{11}$  (a) and inverse Hall conductivity  $1/D_{12}$  (b) as functions of  $(B^2 + \rho^2)^{1/2}$  for fixed ratio  $\rho/B = 0.025$ . (- - -) is the Boltzmann theory, (—) the improved Boltzmann theory, and ( $\diamond$ ) are the simulation data

Fig. 10: Inverse Ohmic conductivity  $1/D_{11}$  (a) and inverse Hall conductivity  $1/D_{12}$  (b) as functions of  $(B^2 + \rho^2)^{1/2}$  for fixed ratio  $\rho/B = 0.1$ . (- - -) is the Boltzmann theory, (—) the improved Boltzmann theory, and ( $\diamond$ ) are the simulation data

Fig. 11: Real part of  $\hat{C}_{11}(\omega)$  with  $\rho/B = 0.025$  and  $(B^2 + \rho^2)^{1/2} = 0.105$  from the improved Boltzmann theory (a) and from the simulation data (b)

Fig. 12: Negative imaginary part of  $\hat{C}_{12}(\omega)$  with  $\rho/B = 0.025$  and  $(B^2 + \rho^2)^{1/2} = 0.105$  from the improved Boltzmann theory (a) and from the simulation data (b)



Fig. 13: Integrated velocity autocorrelation functions  $\langle v_1(0)x_1(t) \rangle$  (a) and  $\langle v_1(0)x_2(t) \rangle$  (b) with  $\rho = 0.15$  and  $B = 0.2$  as functions of  $(\tau/t)^{0.9}$

Fig. 14: Integrated velocity autocorrelation functions  $\langle v_1(0)x_1(t) \rangle$  (a) and  $\langle v_1(0)x_2(t) \rangle$  (b) with  $\rho = 0.2$  and  $B = 2.2$  as functions of  $(\tau/t)^{0.4}$

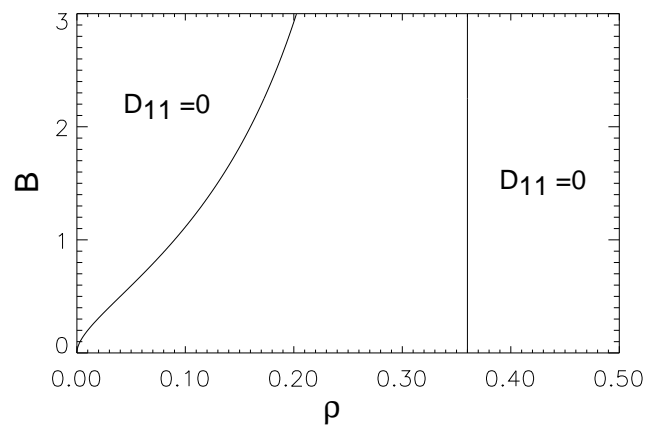


Fig. 1

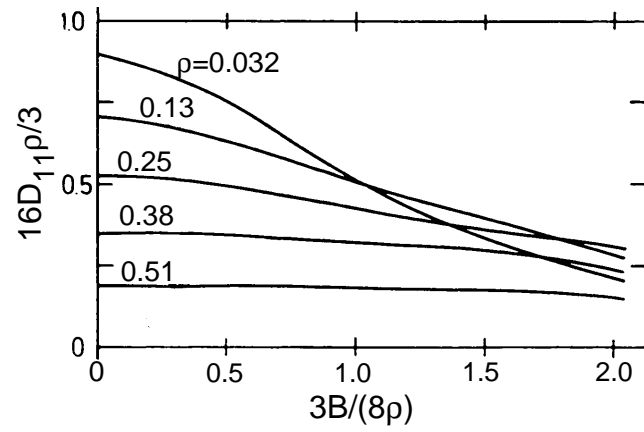


Fig. 6a

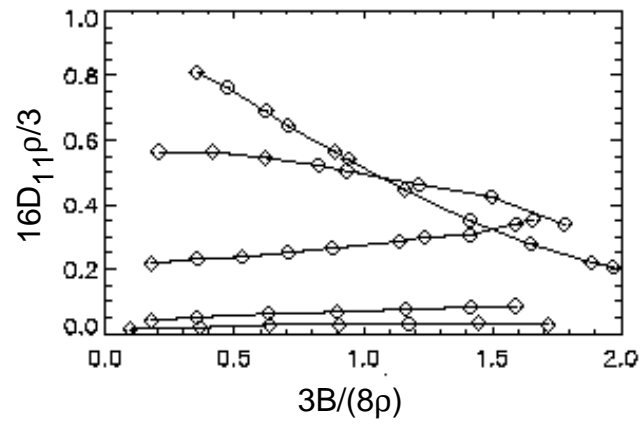


Fig. 6b

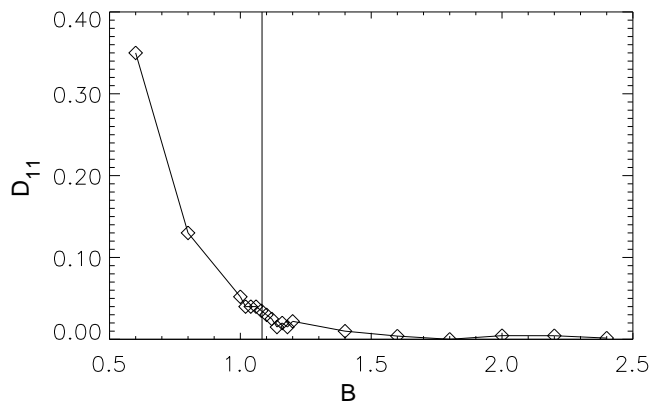


Fig. 2a

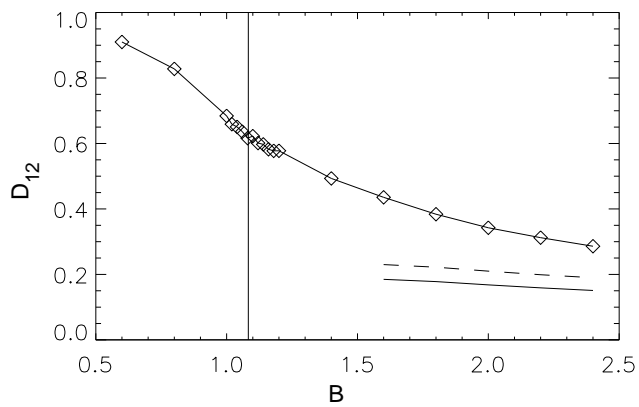


Fig. 2b

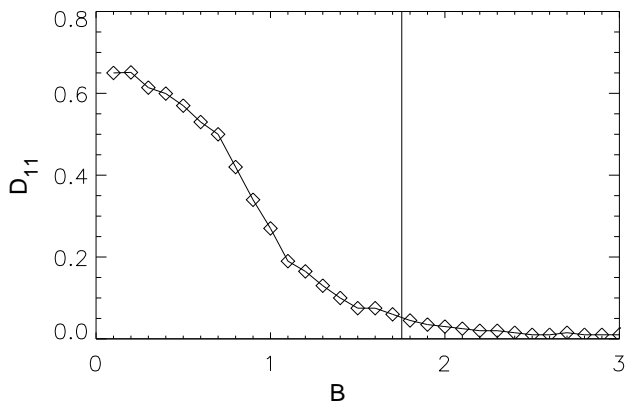


Fig. 3a

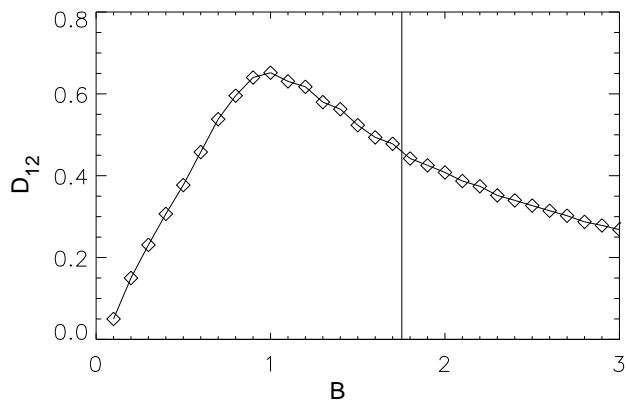


Fig. 3b

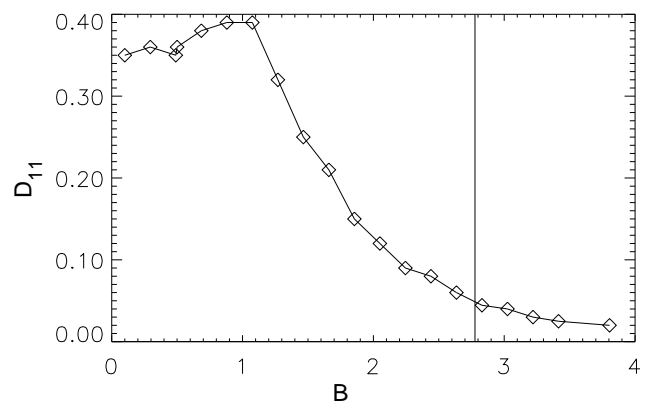


Fig. 4a

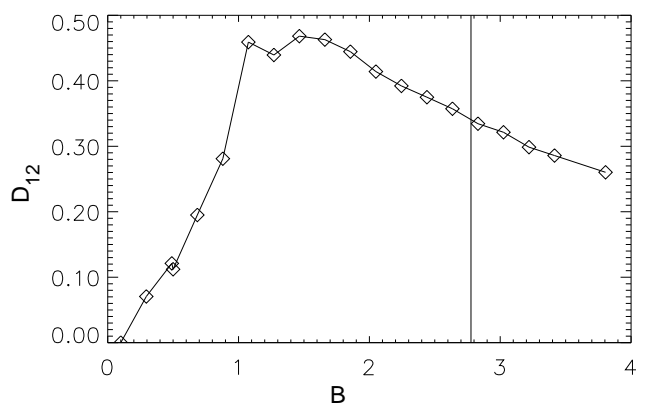


Fig. 4b

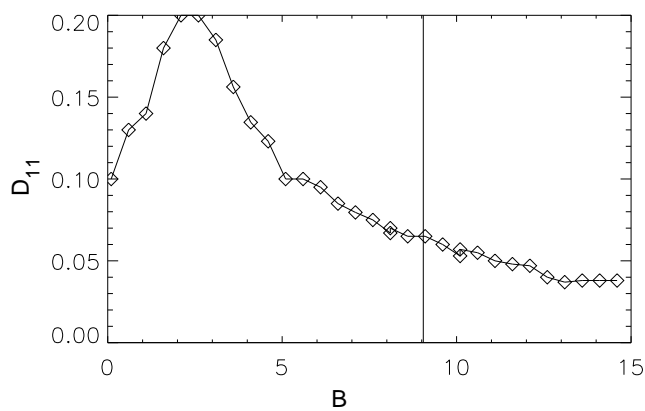


Fig. 5a

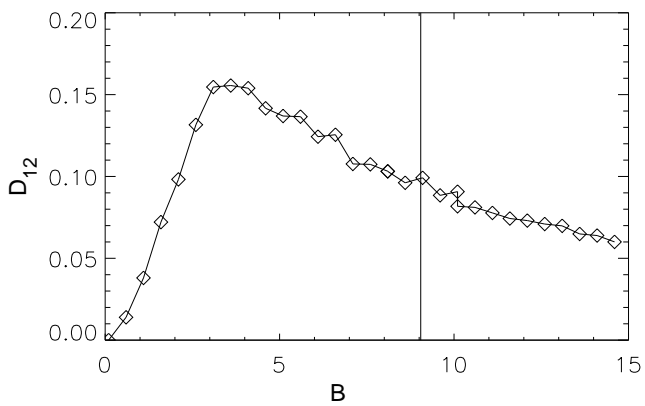


Fig. 5b

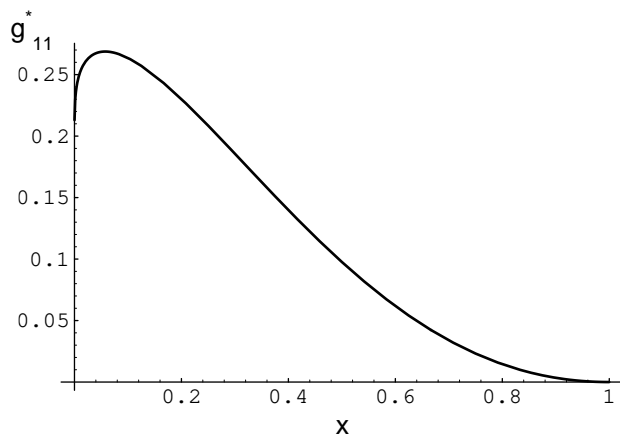


Fig. 7a

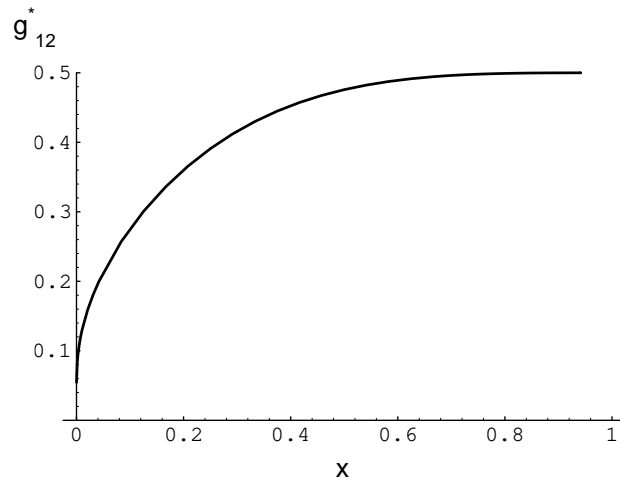


Fig. 7b

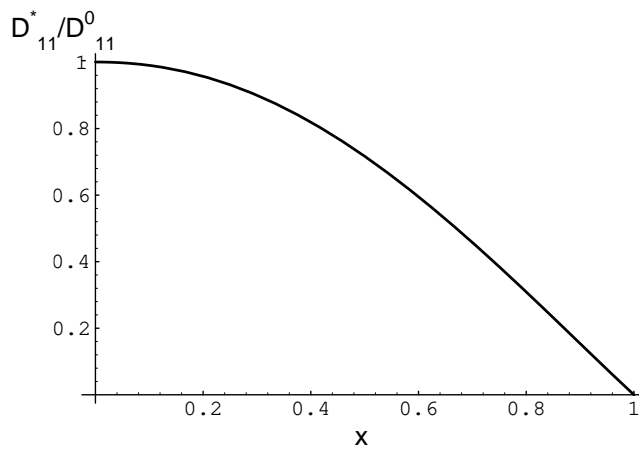


Fig. 8a

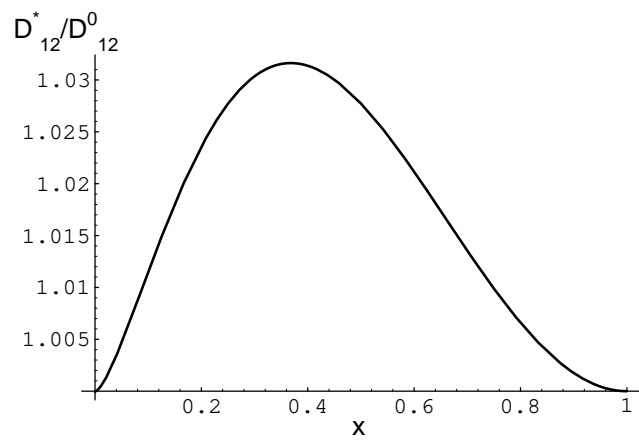


Fig. 8b

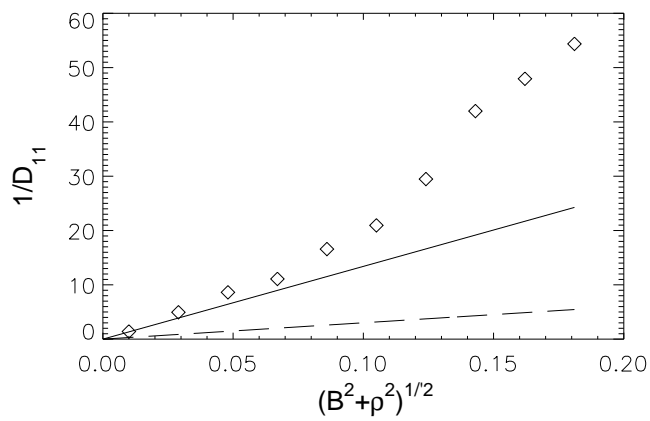


Fig. 9a

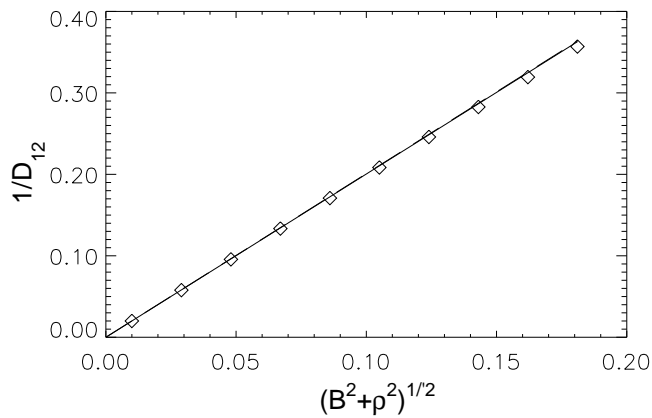


Fig. 9b

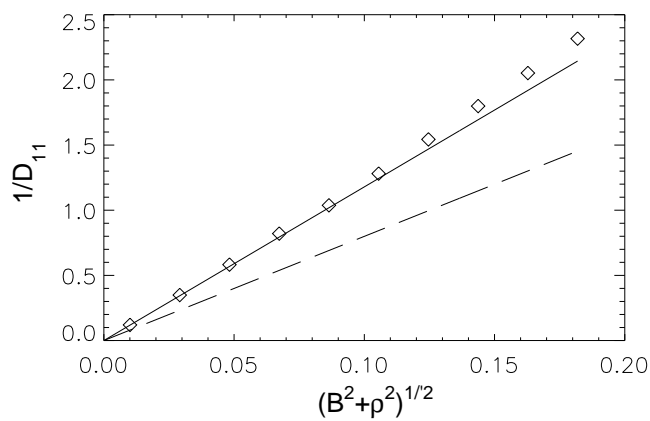


Fig. 10a

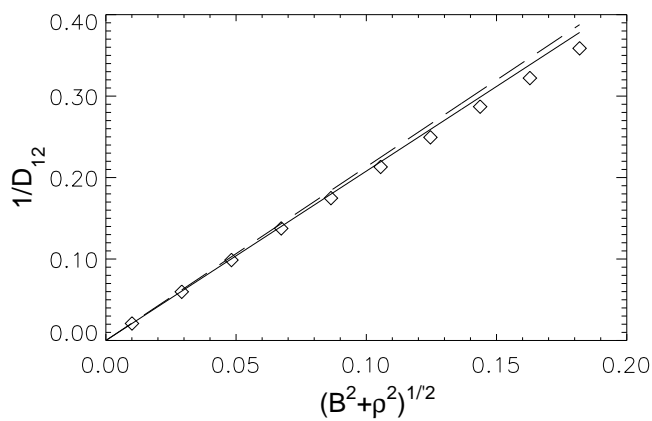


Fig. 10b

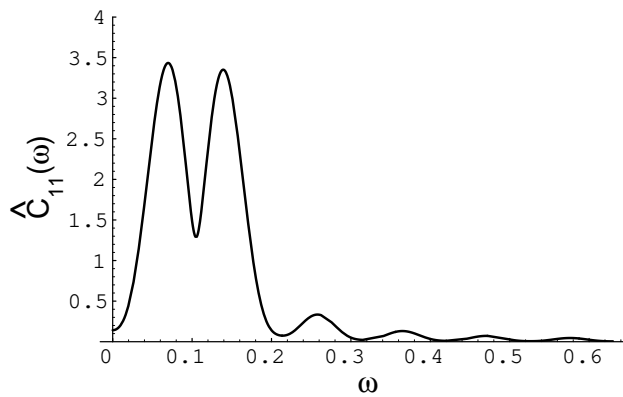


Fig. 11a

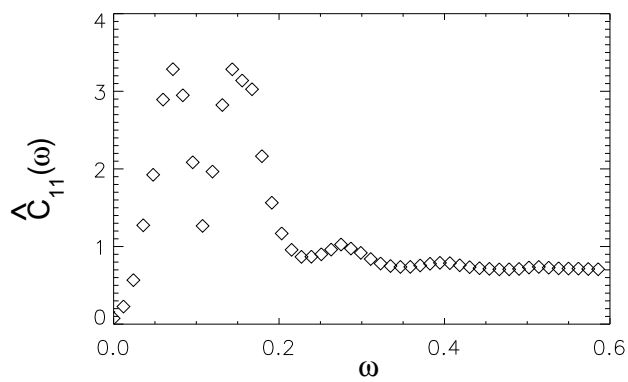


Fig. 11b

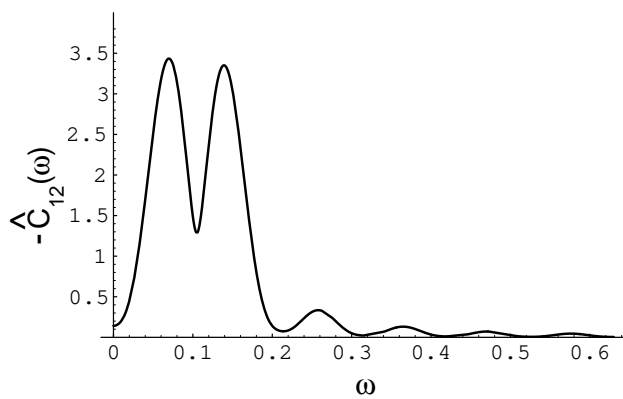


Fig. 12a

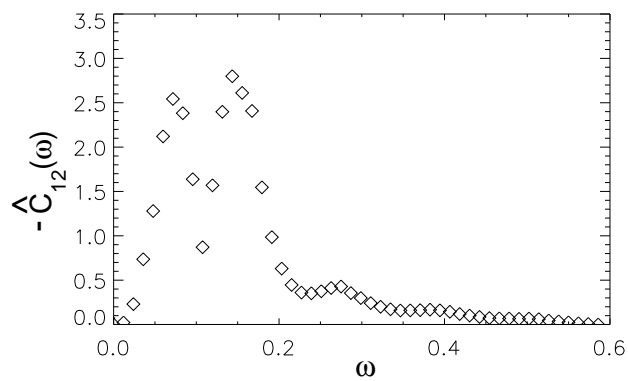


Fig. 12b

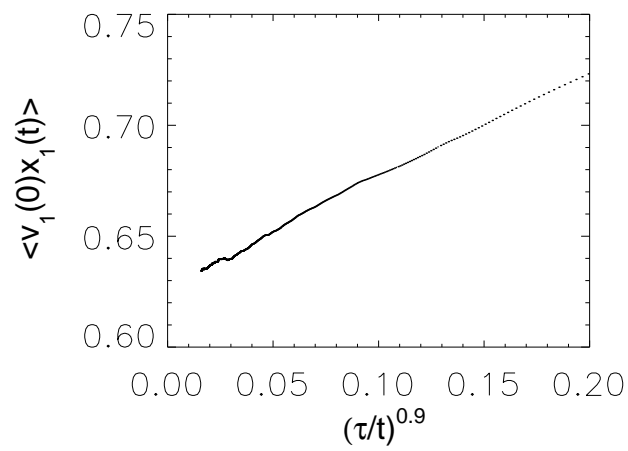


Fig. 13a

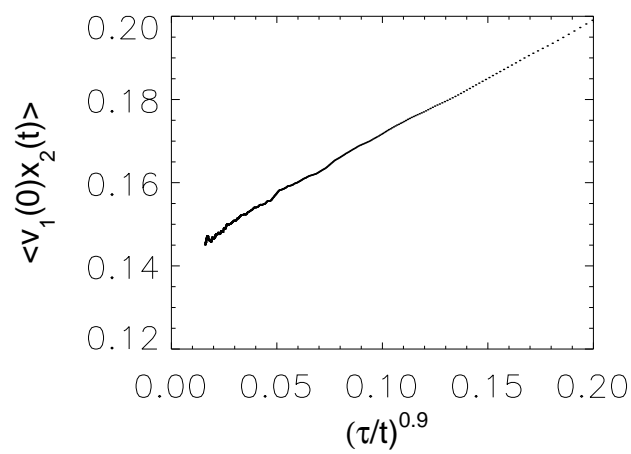


Fig. 13b

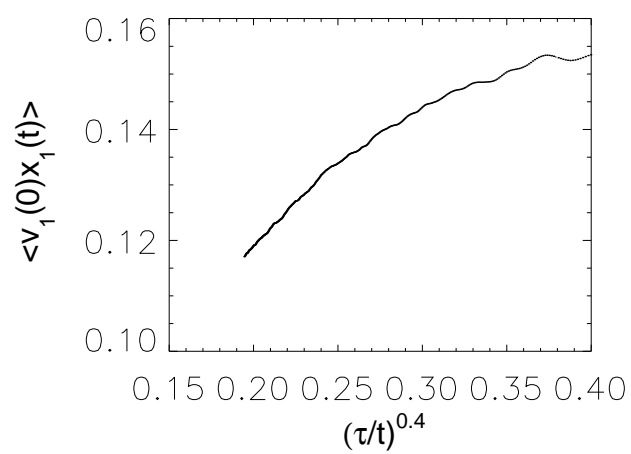


Fig. 14a

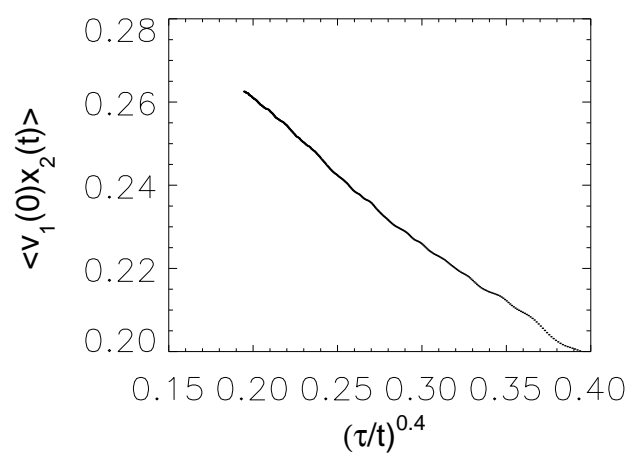


Fig. 14b